European Journal of Mechanics B/Fluids 48 (2014) 174–182

Contents lists available at ScienceDirect

European Journal of Mechanics B/Fluids

journal homepage: www.elsevier.com/locate/ejmflu

Pulsating flow of an incompressible micropolar fluid between permeable beds with an inclined uniform magnetic field

Punnamchandar Bitla [a,*], T.K.V. Iyengar [b]

[a] Department of Mathematics, Amrita Vishwa Vidyapeetham, Coimbatore, 641112, India
[b] Department of Mathematics, National Institute of Technology Warangal, 506004, India

ARTICLE INFO

Article history:
Received 10 May 2012
Received in revised form
13 May 2014
Accepted 2 June 2014
Available online 16 June 2014

Keywords:
Pulsating flow
Micropolar fluid
Microrotation
Darcy's law
Fluid–permeable bed interface
Inclined magnetic field

ABSTRACT

In this paper, we investigate the pulsating flow of an incompressible and slightly conducting micropolar fluid between two homogeneous permeable beds in the presence of an inclined uniform magnetic field. The flow between the permeable beds is assumed to be governed by Eringen's micropolar fluid flow equations and that in the permeable beds by Darcy's law with the Beavers–Joseph slip conditions at the fluid–permeable bed interfaces. It is assumed that a uniform magnetic field is applied at an angle θ with the y-axis. The equations are solved analytically and the expressions for velocity and microrotation are obtained. The effects of the magnetic parameter and the other material parameters are studied numerically and the results are presented through graphs.

1. Introduction

Pulsating flow is a periodic flow that oscillates around non-zero mean value. The severity of pulsating flow depends on pulsation amplitudes, frequency and waveform. A complete treatment of the fluid dynamics of steady and pulsatory flow with emphasis on basic mechanics, physics and applications can be seen in [1]. Carpinlioglu and Gundogdu [2] presented a review on the pulsatile pipe flow studies directing towards future research topics. Pulsating flow is generally encountered in natural systems such as human respiratory, circulatory and vascular systems and in engineering systems such as internal combustion engines, thermoacoustic coolers, Stirling engines, bio-reactors and MEMS microfluidic engineering applications.

The laminar flows in channels with permeable walls have gained considerable attention because of their applications in modelling pulsating diaphragms, filtration, and grain regression during solid propellant combustion. Wang [3] studied the pulsatile flow in a porous channel. Vajravelu et al. [4] studied the pulsatile flow between permeable beds. Malathy and Srinivas [5] studied the pulsating flow of a viscous, incompressible, Newtonian fluid between permeable beds under the influence of transverse magnetic field. Ramakrishnan and Shailendhra [6] studied hydromagnetic steady flow through uniform channel bounded by porous media. Avinash et al. [7] studied the pulsatile flow of a viscous stratified fluid of variable viscosity between permeable beds. Iyengar and Punnamchandar [8,9] studied pulsating flows of couple stress fluid and micropolar fluid between two parallel permeable beds in the absence of magnetic effects.

To the extent the present authors have surveyed the pulsatile flow of an incompressible micropolar fluid between two permeable beds with an inclined uniform magnetic field has not been studied so far. The micropolar fluid model introduced by [10] can be used to explain the flow of liquid crystals with rigid molecules, magnetic fluids, biological fluids, lubricants, polymeric additives, geomorphological sediments, colloidal suspensions, haematological suspensions etc. In such fluids the micro-elements possess both translational and rotational motions. The interaction of the velocity field and microrotation field can be described through new material constants in addition to those of a classical Newtonian fluid. Eringen's micropolar fluid model includes the classical Navier–Stokes equations as a special case and can cover both the theory and applications, many more phenomena than the classical model can. Extensive reviews of the theory and applications of micropolar fluids can be found in the books by [11,12].

In this paper, we study the flow of an incompressible micropolar fluid between permeable beds with an inclined uniform

* Corresponding author. Tel.: +91 9030859034.
E-mail addresses: punnam.nitw@gmail.com, b_punnamchandar@cb.amrita.edu (P. Bitla), iyengar.tkv@gmail.com (T.K.V. Iyengar).

http://dx.doi.org/10.1016/j.euromechflu.2014.06.002
0997-7546/

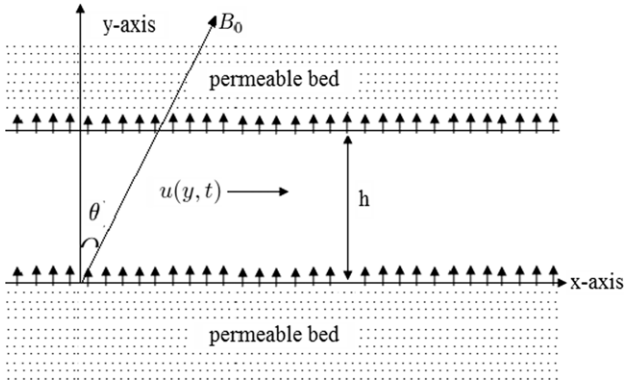

Fig. 1. Flow diagram.

magnetic field. The flow is assumed to be driven by an unsteady pulsating pressure gradient. The flow through the permeable beds is assumed to be governed by Darcy's law and the flow between the permeable beds by Eringen's micropolar fluid flow equations. The Beavers–Joseph (BJ) slip boundary conditions are used at the interfaces of the permeable beds [13]. The equations are solved analytically and the expressions for velocity and microrotation are obtained. The effects of micropolar parameters, Hartmann number, angle of inclination of the uniform magnetic field, porosity parameter, frequency parameter and steady and oscillatory components of the pressure gradient on the velocity and microrotation are studied numerically and the results are presented through graphs.

2. Mathematical formulation

The field equations describing a micropolar fluid flow are [10]

$$\frac{\partial \rho}{\partial t} + \nabla.(\rho \bar{q}) = 0 \tag{1}$$

$$\rho \frac{d\bar{q}}{dt} = \rho \bar{f} - \nabla p + \kappa \nabla \times \bar{v} - (\mu + \kappa)(\nabla \times \nabla \times \bar{q}) + (\lambda + 2\mu + \kappa)\nabla(\nabla.\bar{q}) + \bar{J} \times \bar{B} \tag{2}$$

$$\rho j \frac{d\bar{v}}{dt} = \rho \bar{l} - 2\kappa \bar{v} + \kappa \nabla \times \bar{q} - \gamma(\nabla \times \nabla \times \bar{v}) + (\alpha_1 + \beta + \gamma)\nabla(\nabla.\bar{v}) \tag{3}$$

where $\bar{q}$ and $\bar{v}$ are velocity and microrotation vectors respectively. J is the current density and B is the total magnetic field which is the sum of the applied and induced magnetic fields. $\bar{f}, \bar{l}$ are the body force per unit mass and body couple per unit mass respectively and p is the pressure at any point. ρ and j are the density of the fluid and gyration parameter respectively and are assumed to be constant. The material quantities (λ, μ, κ) are viscosity coefficients and $(\alpha_1, \beta, \gamma)$ are gyroviscosity coefficients satisfying the constraints

$$\begin{aligned} &\kappa \geq 0; \quad 2\mu + \kappa \geq 0; \quad 3\lambda + 2\mu + \kappa \geq 0; \\ &\gamma \geq 0; \quad |\beta| \leq \gamma; \quad 3\alpha_1 + \beta + \gamma \geq 0. \end{aligned} \tag{4}$$

We consider the pulsating flow of an incompressible, slightly conducting micropolar fluid between two permeable beds. The permeable beds are rigid and homogeneous. Fig. 1 shows the physical model of the problem under consideration. The Cartesian coordinate system is chosen in such a way that the x-axis is taken along the interface of the lower permeable bed and the y-axis normal to it. Let $y = 0$ and $y = h$ represent the interfaces of the permeable beds. The fluid is injected into the channel from the lower permeable bed with a velocity V and is sucked into the upper permeable bed with the same velocity. The permeabilities of lower and upper beds are k_1 and k_2 respectively. The flow in upper and lower permeable beds is assumed to be governed by Darcy's law. The flow between the permeable beds is assumed to be governed by micropolar fluid flow equations. The thickness of the permeable beds is much larger than the width of the channel so that we can directly use Beavers–Joseph condition at the interfaces of the channel. A uniform magnetic field of strength B_o is applied at an angle θ with the y-axis. The induced magnetic field can be neglected in comparison with the applied magnetic field, as magnetic Reynolds number is much less than unity [14,15]. The fluid is driven by a pulsating pressure gradient given by

$$-\frac{\partial p}{\partial x} = \left(\frac{\partial p}{\partial x}\right)_s + \left(\frac{\partial p}{\partial x}\right)_o e^{i\omega t} \tag{5}$$

where $\left(\frac{\partial p}{\partial x}\right)_s$ and $\left(\frac{\partial p}{\partial x}\right)_o$ are steady and oscillatory components of the pressure gradient respectively and ω is the frequency.

Under the assumptions, we have $\bar{q} = (u(y,t), V, 0)$ and $\bar{v} = (0, 0, c(y,t))$. With this, the governing fluid flow equations of the problem in the absence of body forces and body couples are given by

$$\rho\left(\frac{\partial u}{\partial t} + V\frac{\partial u}{\partial y}\right) = -\frac{\partial p}{\partial x} + \kappa\frac{\partial c}{\partial y} + (\mu + \kappa)\frac{\partial^2 u}{\partial y^2} - \sigma_e(B_0 \cos\theta)^2 u \tag{6}$$

$$\rho j\left(\frac{\partial c}{\partial t} + V\frac{\partial c}{\partial y}\right) = -2\kappa c - \kappa\frac{\partial u}{\partial y} + \gamma\frac{\partial^2 c}{\partial y^2}. \tag{7}$$

Herein the velocity component $u(y,t)$ is to satisfy the conditions

$$\left.\begin{aligned} \frac{\partial u}{\partial y} &= \frac{\alpha}{\sqrt{k_1}}(u_{B_1} - Q_1) \quad \text{at } y = 0 \\ \frac{\partial u}{\partial y} &= -\frac{\alpha}{\sqrt{k_2}}(u_{B_2} - Q_2) \quad \text{at } y = h \end{aligned}\right\} \tag{8}$$

and the microrotation component $c(y,t)$ is to satisfy the condition

$$c = 0 \quad \text{at } y = 0 \quad \text{and} \quad y = h \tag{9}$$

where σ_e is the electrical conductivity and B_o is the applied magnetic field. $u_{B_1} = u|_{y=0}$ and $u_{B_2} = u|_{y=h}$ are the slip velocities at the interfaces of the lower and upper permeable beds respectively. α is the slip parameter. $Q_1 = -\frac{k_1}{\mu}\frac{\partial p}{\partial x}$ and $Q_2 = -\frac{k_2}{\mu}\frac{\partial p}{\partial x}$ are Darcy's velocities in the lower and upper permeable beds respectively. Eq. (8) represents the BJ slip conditions. Eq. (9) stipulates that the microrotation vanishes at the interfaces of the permeable beds.

In view of the pulsating pressure gradient, let us assume that the velocity and microrotation are in the form

$$u(y,t) = u_s(y) + u_o(y)e^{i\omega t} \tag{10}$$

$$c(y,t) = c_s(y) + c_o(y)e^{i\omega t} \tag{11}$$

where u_s and c_s represent steady parts and u_o and c_o represent the oscillatory parts of the velocity and microrotation respectively.

The following non-dimensionalization scheme is introduced to make the governing equations and the boundary conditions dimensionless.

$$\begin{aligned} &u^* = \frac{u}{V}, \quad u_s{}^* = \frac{u_s}{V}, \quad u_o{}^* = \frac{u_o}{V}, \\ &c^* = \frac{ch}{V}, \quad c_s{}^* = \frac{c_s h}{V}, \quad c_o{}^* = \frac{c_o h}{V}, \quad u_{B_1}^* = \frac{u_{B_1}}{V}, \\ &u_{B_2}^* = \frac{u_{B_2}}{V}, \quad p^* = \frac{p}{\rho V^2}, \quad \omega^* = \frac{\omega h}{V}, \\ &t^* = \frac{tV}{h}, \quad x^* = \frac{x}{h}, \quad y^* = \frac{y}{h}. \end{aligned} \tag{12}$$

The equations and boundary conditions governing the non-dimensionalized pulsating flow are given by

$$\frac{\partial^2 u}{\partial y^2} + m\frac{\partial c}{\partial y} - R\left(\frac{\partial u}{\partial y} + \frac{\partial u}{\partial t}\right) - (M\cos\theta)^2 u = R\left(\frac{\partial p}{\partial x}\right) \tag{13}$$

$$\frac{\partial^2 c}{\partial y^2} - n\frac{\partial u}{\partial y} - RP_j\left(\frac{\partial c}{\partial y} + \frac{\partial c}{\partial t}\right) - 2nc = 0 \tag{14}$$

after dropping $*$'s.

The non-dimensionalized boundary conditions on u and c are

$$\left.\begin{aligned} \frac{\partial u}{\partial y} &= \alpha\sigma_1\left(u_{B_1} - \frac{R}{(1-m)\sigma_1^2}\frac{\partial p}{\partial x}\right) \quad \text{at } y = 0 \\ \frac{\partial u}{\partial y} &= -\alpha\sigma_2\left(u_{B_2} - \frac{R}{(1-m)\sigma_2^2}\frac{\partial p}{\partial x}\right) \quad \text{at } y = 1 \end{aligned}\right\} \tag{15}$$

$$c = 0 \quad \text{at } y = 0 \text{ and } 1 \tag{16}$$

where $u = u_s + u_o e^{i\omega t}$, $c = c_s + c_o e^{i\omega t}$, $u_{B_1} = u_{s_{B1}} + u_{o_{B1}} e^{i\omega t}$, $u_{B_2} = u_{s_{B2}} + u_{o_{B2}} e^{i\omega t}$, $-\frac{\partial p}{\partial x} = \left(\frac{\partial p}{\partial x}\right)_s + \left(\frac{\partial p}{\partial x}\right)_o e^{i\omega t}$, Reynolds number $R = \frac{\rho V h}{\mu+\kappa}$, Hartmann number $M = B_0 h\sqrt{\frac{\sigma_e}{\mu}}$, coupling parameter $m = \frac{\kappa}{\mu+\kappa}$, gyration parameter $n = \frac{\kappa h^2}{\gamma}$, microinertia parameter $P_j = \frac{j(\mu+\kappa)}{\gamma}$ and porosity parameters: $\sigma_1 = \frac{h}{\sqrt{k_1}}$, $\sigma_2 = \frac{h}{\sqrt{k_2}}$.

Steady part

The governing equations of the steady part are given by

$$\frac{d^2 u_s}{dy^2} + m\frac{dc_s}{dy} - R\frac{du_s}{dy} - (M\cos\theta)^2 u_s = -R\Pi_s \tag{17}$$

$$\frac{d^2 c_s}{dy^2} - n\frac{du_s}{dy} - RP_j\frac{dc_s}{dy} - 2nc_s = 0. \tag{18}$$

The boundary conditions to be satisfied by u_s and c_s are

$$\left.\begin{aligned} \frac{du_s}{dy} &= \alpha\sigma_1\left(u_{sB_1} - \frac{R\Pi_s}{(1-m)\sigma_1^2}\right) \quad \text{at } y = 0 \\ \frac{du_s}{dy} &= -\alpha\sigma_2\left(u_{sB_2} - \frac{R\Pi_s}{(1-m)\sigma_2^2}\right) \quad \text{at } y = 1 \end{aligned}\right\} \tag{19}$$

$$c_s = 0 \quad \text{at } y = 0 \text{ and } 1 \tag{20}$$

where $\Pi_s = \left(\frac{\partial p}{\partial x}\right)_s$.

Oscillatory part

The governing equations of the oscillatory part are given by

$$\frac{d^2 u_o}{dy^2} + m\frac{dc_o}{dy} - R\frac{du_o}{dy} - ((M\cos\theta)^2 + i\omega R)u_o = -R\Pi_o \tag{21}$$

$$\frac{d^2 c_o}{dy^2} - n\frac{du_o}{dy} - RP_j\frac{dc_o}{dy} - (2n + i\omega RP_j)c_o = 0. \tag{22}$$

The boundary conditions to be satisfied by u_o and c_o are

$$\left.\begin{aligned} \frac{du_o}{dy} &= \alpha\sigma_1\left(u_{oB_1} - \frac{R\Pi_o}{(1-m)\sigma_1^2}\right) \quad \text{at } y = 0 \\ \frac{du_o}{dy} &= -\alpha\sigma_2\left(u_{oB_2} - \frac{R\Pi_o}{(1-m)\sigma_2^2}\right) \quad \text{at } y = 1 \end{aligned}\right\} \tag{23}$$

$$c_o = 0 \quad \text{at } y = 0 \text{ and } 1 \tag{24}$$

where $\Pi_o = \left(\frac{\partial p}{\partial x}\right)_o$.

3. Solution of the problem

Solution of the steady part

From Eqs. (17) and (18), we see that $u_o(y)$ satisfies the fourth order ordinary differential equation

$$u_s^{iv} - A_s u_s''' + B_s u_s'' + C_s u_s' + D_s u_s = 2nR\Pi_s \tag{25}$$

where the expressions for A_s, B_s, C_s and D_s are given in Appendix A.

The solution of Eq. (25) is of the form

$$u_s(y) = C_1 e^{\lambda_1 y} + C_2 e^{\lambda_2 y} + C_3 e^{\lambda_3 y} + C_4 e^{\lambda_4 y} + 2nR\Pi_s/D_s. \tag{26}$$

By using Eqs. (17) and (18), we get $c_s(y)$ in terms of $u_s(y)$ as given by

$$c_s(y) = \frac{1}{2nm}\left[-u_s''' + A_s u_s'' - (B_s + 2n)u_s' - RP_j((M\cos\theta)^2 u_s - R\Pi_s)\right]. \tag{27}$$

Using this and the expression for $u_s(y)$ given in Eq. (26), we get the expression for $c_s(y)$ as

$$c_s(y) = D_1 e^{\lambda_1 y} + D_2 e^{\lambda_2 y} + D_3 e^{\lambda_3 y} + D_4 e^{\lambda_4 y}. \tag{28}$$

The solution of the steady part described in Section 2 is given by

$$u_s(y) = C_1 e^{\lambda_1 y} + C_2 e^{\lambda_2 y} + C_3 e^{\lambda_3 y} + C_4 e^{\lambda_4 y} + 2nR\Pi_s/D_s \tag{29}$$

$$c_s(y) = D_1 e^{\lambda_1 y} + D_2 e^{\lambda_2 y} + D_3 e^{\lambda_3 y} + D_4 e^{\lambda_4 y} \tag{30}$$

where C_j ($j = 1$–4) and D_j ($j = 1$–4) are determined by using the boundary conditions given by Eqs. (19) and (20). The actual expressions for λ_j ($j = 1$–4), C_j ($j = 1$–4) and D_j ($j = 1$–4) are given in Appendix A.

Solution of the oscillatory part

From Eqs. (21) and (22), we see that $u_o(y)$ satisfies the fourth order ordinary differential equation

$$u_o^{iv} - Au_o''' + Bu_o'' + Cu_o' + Du_o = bR\Pi_o \tag{31}$$

where the expressions for A, B, C and D are given in Appendix B.

The solution of Eq. (31) is of the form

$$u_o(y) = C_5 e^{\lambda_5 y} + C_6 e^{\lambda_6 y} + C_7 e^{\lambda_7 y} + C_8 e^{\lambda_8 y} + R\Pi_o/a. \tag{32}$$

By using Eqs. (21) and (22), we get $c_o(y)$ in terms of $u_o(y)$ as given by

$$c_o(y) = \frac{1}{mb}\left[-u_o''' + Au_o'' - (B + b)u_o' - RP_j(au_o - R\Pi_o)\right]. \tag{33}$$

Using this and the expression for $u_o(y)$ given in Eq. (32), we get the expression for $c_o(y)$ as

$$c_o(y) = D_5 e^{\lambda_5 y} + D_6 e^{\lambda_6 y} + D_7 e^{\lambda_7 y} + D_8 e^{\lambda_8 y}. \tag{34}$$

The solution of the oscillatory part described in Section 2 is given by

$$u_o(y) = C_5 e^{\lambda_5 y} + C_6 e^{\lambda_6 y} + C_7 e^{\lambda_7 y} + C_8 e^{\lambda_8 y} + R\Pi_o/a \tag{35}$$

$$c_o(y) = D_5 e^{\lambda_5 y} + D_6 e^{\lambda_6 y} + D_7 e^{\lambda_7 y} + D_8 e^{\lambda_8 y} \tag{36}$$

where C_j ($j = 5$–8) and D_j ($j = 5$–8) are determined by using the boundary conditions given by Eqs. (23) and (24). The actual expressions for λ_j ($j = 5$–8), C_j ($j = 5$–8) and D_j ($j = 5$–8) are given in Appendix B.

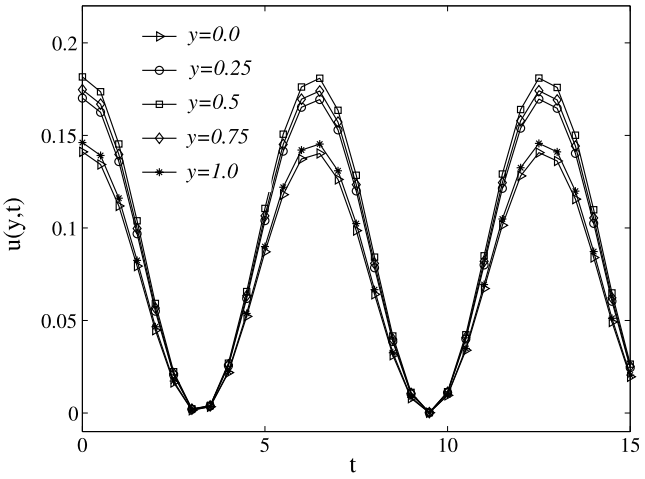

Fig. 2. Variation of $u(y, t)$ for $\alpha = 0.5, R = 0.5, M = 2, \theta = \pi/6, \sigma = 5, \Pi_s = \Pi_o = 1, P_j = 1, m = 0.5, n = 0.5$.

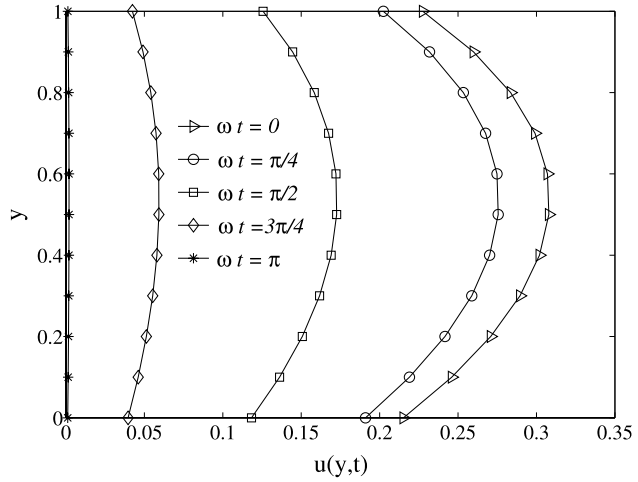

Fig. 3. Effect of ωt on $u(y, t)$ for $\alpha = 0.5, R = 0.5, M = 2, \theta = \pi/6, \sigma = 5, \Pi_s = \Pi_o = 1, P_j = 1, m = 0.5, n = 0.5$.

Solution of the pulsating flow

The solution of the pulsating flow is given by

$$u(y, t) = u_s(y) + u_o(y)e^{i\omega t} \tag{37}$$

$$c(y, t) = c_s(y) + c_o(y)e^{i\omega t} \tag{38}$$

where $u_s(y)$, $c_s(y)$ and $u_o(y)$, $c_o(y)$ are known from the steady part and oscillatory part solutions given in Eqs. (29), (30), (35) and (36) respectively.

4. Results and discussion

Under the assumption that both the permeable beds have different permeabilities, the analytical solutions for velocity and microrotation profiles for pulsating flows are derived. In the numerical work, we have taken that both the permeable beds have the same permeability, i.e., $k_1 = k_2 = k(\sigma_1 = \sigma_2 = \sigma)$.

The effects of various parameters entering into the problem on pulsating velocity $u(y, t)$ are depicted in Figs. 2–12. Fig. 2 shows the variation of the pulsating velocity with respect to t. At $y = 0$ and $y = 1$, the velocities correspond to the slip velocities at the interfaces of the lower and upper permeable beds respectively. Fig. 3 shows the variation of the pulsating velocity with respect to ωt. As ωt is increasing, the velocity is decreasing.

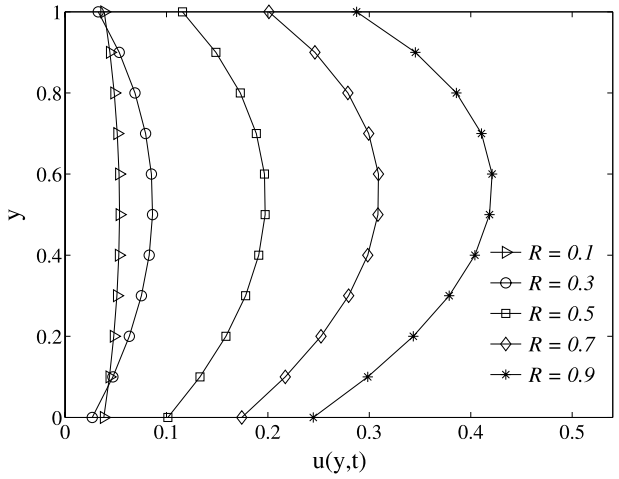

Fig. 4. Effect of R on $u(y, t)$ for $\alpha = 0.5, M = 2, \theta = \pi/6, \sigma = 5, \omega t = \pi/4, \Pi_s = \Pi_o = 1, P_j = 1, m = 0.5, n = 0.5$.

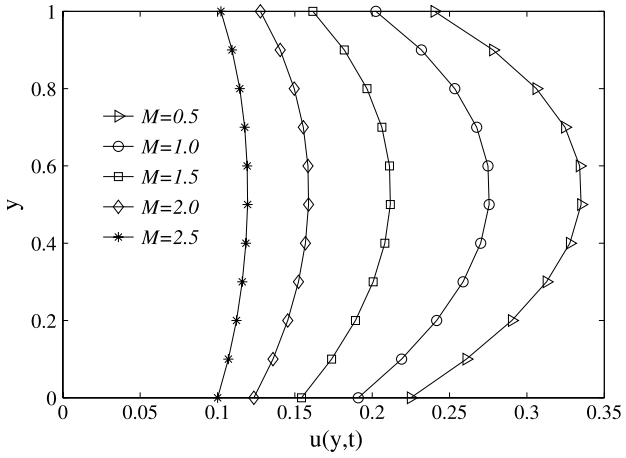

Fig. 5. Effect of M on $u(y, t)$ for $\alpha = 0.5, R = 0.5, \theta = \pi/6, \sigma = 5, \omega t = \pi/4, P_j = 1, \Pi_s = \Pi_o = 1, m = 0.5, n = 0.5$.

From Fig. 4, we notice that as Reynolds number R is increasing, the velocity is increasing. The effect of Hartmann number (magnetic parameter) M on the velocity is shown in Fig. 5. As M is increasing, it is seen that the velocity is decreasing. This shows that the imposed magnetic field has a retarding influence on the flow. Fig. 6 shows the effect of the inclination angle θ $(0 \leq \theta < \pi/2)$ on the pulsating velocity profile. As θ is increasing, the velocity is increasing. Here $\theta = 0$ corresponds to the magnetic field applied normal to the direction of the flow. As $\theta \to \pi/2$, the magnetic field is in the flow direction which corresponds to the pulsating flow in the absence of magnetic field (i.e., $(M \cos\theta)^2 \to 0$).

In Fig. 7 we see the effect of the microinertia parameter P_j on the pulsating velocity profile. As P_j is increasing, the velocity is increasing. Fig. 8 depicts the variation of velocity with respect to the coupling parameter m $(0 \leq m < 1)$. As m is increasing, the velocity is decreasing. Fig. 9 shows the variation of the pulsating velocity with respect to the gyration parameter n. As n is increasing, nearer to the beds there is no significant change in the velocity whereas it shows a slightly increasing trend in the region between $y = 0.3$ and $y = 0.8$.

Fig. 10 shows the variation of velocity with respect to the porosity parameter σ. It is observed that as σ is increasing, the velocity is decreasing. Figs. 11 and 12 show the effects of steady and oscillatory components of the pressure gradient on the velocity profile respectively. In both the cases, as the magnitude of the pressure gradient increases, the velocity increases.

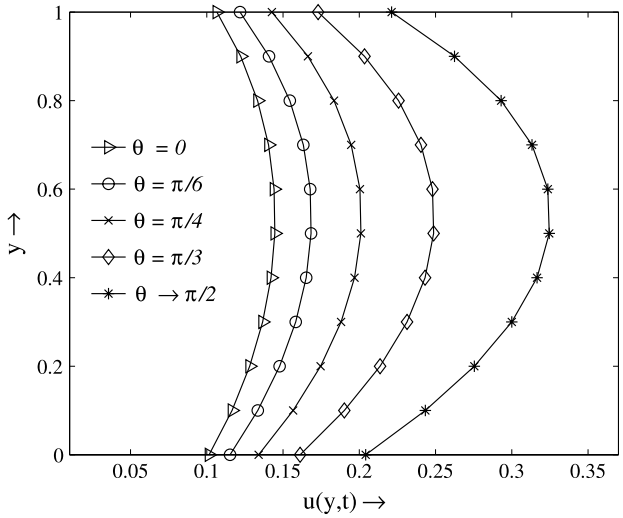

Fig. 6. Effect of θ on $u(y,t)$ for $\alpha = 0.5, R = 0.5, M = 2, \sigma = 5, \Pi_s = \Pi_o = 1, P_j = 1, m = 0.5, n = 0.5$.

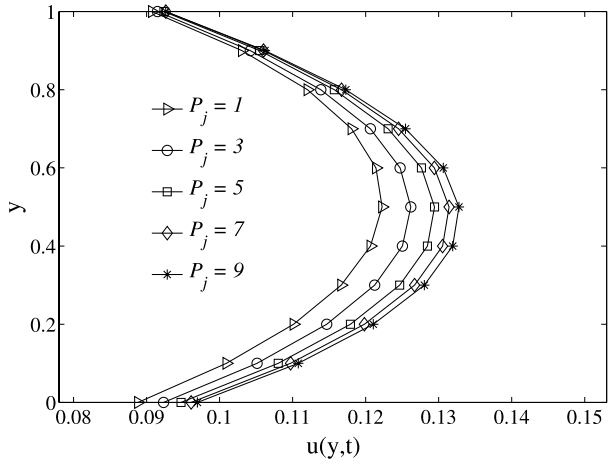

Fig. 7. Effect of P_j on $u(y,t)$ for $\alpha = 0.5, R = 0.5, M = 2, \theta = \pi/6, \sigma = 5, \omega t = \pi/4, \Pi_s = \Pi_o = 1, m = 0.5, n = 0.5$.

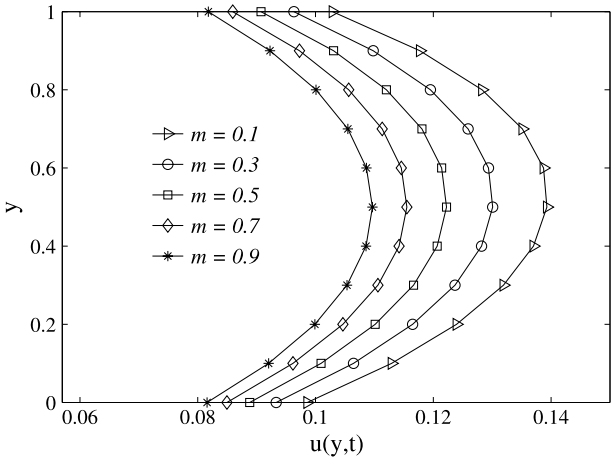

Fig. 8. Effect of m on $u(y,t)$ for $\alpha = 0.5, R = 0.5, M = 2, \theta = \pi/6, \sigma = 5, \omega t = \pi/4, \Pi_s = \Pi_o = 1, P_j = 1, n = 0.5$.

Figs. 13–22 show the effects of various parameters entering into the problem on microrotation $c(y,t)$. The variation of microrotation with respect to ωt is shown in Fig. 13. As ωt is increasing, the

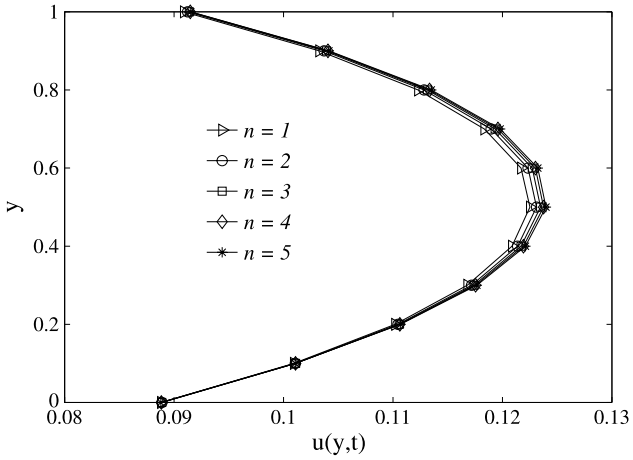

Fig. 9. Effect of n on $u(y,t)$ for $\alpha = 0.5, R = 0.5, M = 2, \theta = \pi/6, \sigma = 5, \omega t = \pi/4, \Pi_s = \Pi_o = 1, P_j = 1, m = 0.5$.

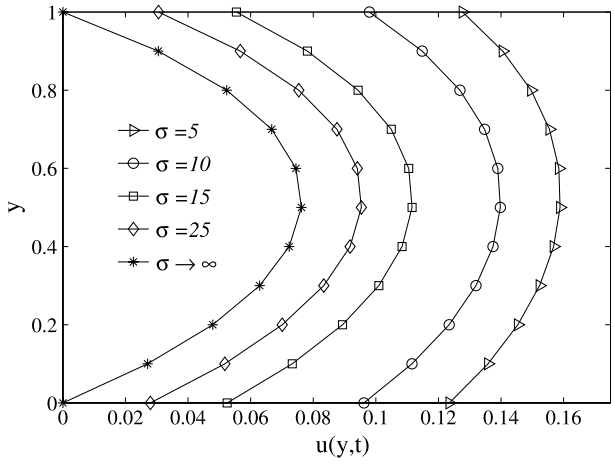

Fig. 10. Effect of σ on $u(y,t)$ for $\alpha = 0.5, R = 0.5, M = 2, \theta = \pi/6, \omega t = \pi/4, \Pi_s = \Pi_o = 1, P_j = 1, m = 0.5, n = 0.5$.

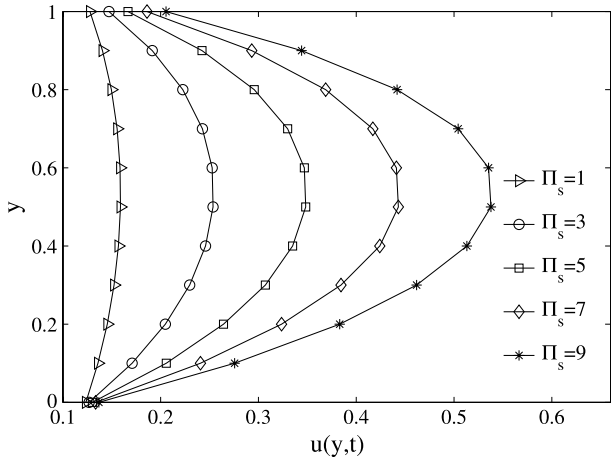

Fig. 11. Effect of Π_s on $u(y,t)$ for $\alpha = 0.5, R = 0.5, M = 2, \theta = \pi/6, \sigma = 5, \omega t = \pi/4, P_j = 1, \Pi_o = 1, m = n = 0.5$.

microrotation is decreasing near the upper permeable bed while it has an increasing trend near the lower permeable bed.

From Fig. 14, we notice that as Reynolds number R is increasing, the microrotation is increasing near the upper permeable bed while it has a decreasing trend at the lower permeable bed. The effect of Hartmann number M on microrotation is shown in Fig. 15.

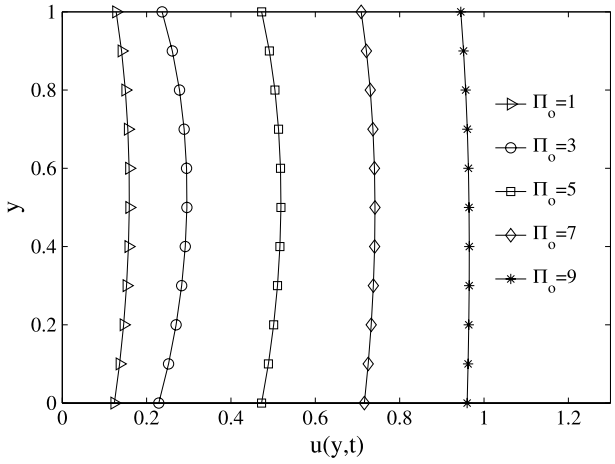

Fig. 12. Effect of Π_o on $u(y,t)$ for $\alpha = 0.5, R = 0.5, M = 2, \theta = \pi/6, \sigma = 5, \omega t = \pi/4, \Pi_s = 1, P_j = 1, m = n = 0.5$.

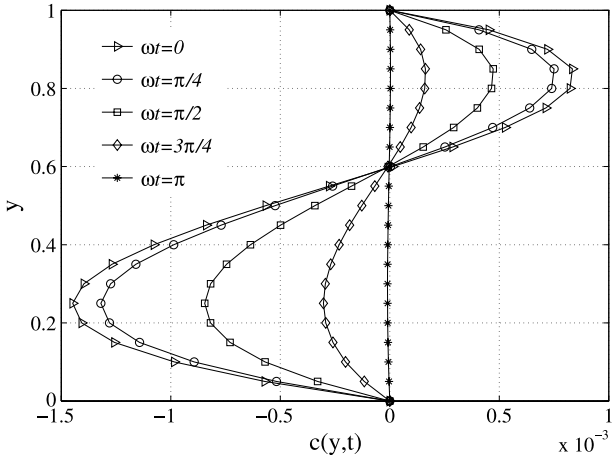

Fig. 13. Effect of ωt on $c(y,t)$ for $\alpha = 0.5, R = 0.5, M = 2, \theta = \pi/6, \sigma = 5, \Pi_s = \Pi_o = 1, P_j = 1, m = 0.5, n = 0.5$.

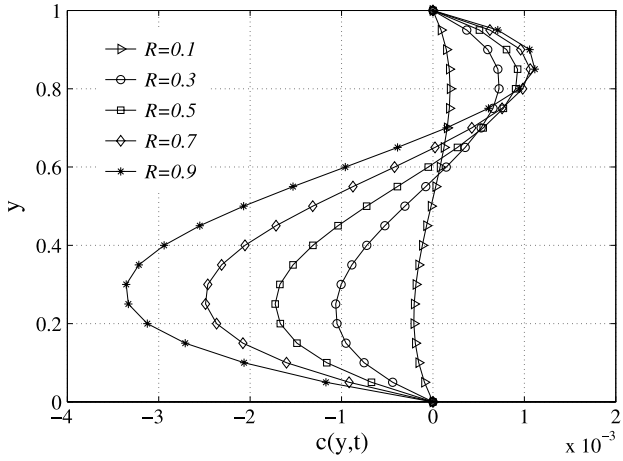

Fig. 14. Effect of R on $c(y,t)$ for $\alpha = 0.5, M = 2, \theta = \pi/6, \sigma = 5, \omega t = \pi/4, \Pi_s = Pi_o = 1, P_j = 1, m = n = 0.5$.

It is seen that as M is increasing, the microrotation is decreasing near the upper permeable bed while it has an increasing trend near the lower permeable bed.

Fig. 16 shows the effect of the inclination angle θ ($0 \leq \theta < \pi/2$) on the microrotation. As θ is increasing, the microrotation is increasing near the upper permeable bed while it has a decreasing trend at the lower permeable bed.

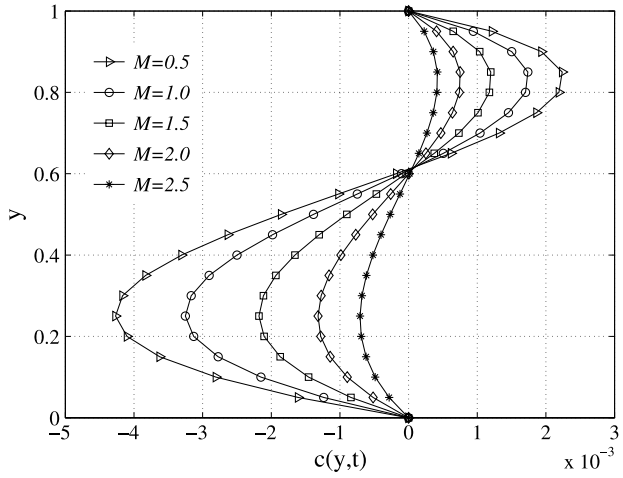

Fig. 15. Effect of M on $c(y,t)$ for $\alpha = 0.5, R = 0.1, \theta = \pi/6, \sigma = 5, \omega t = \pi/4, \Pi_s = \Pi_o = 1, P_j = 1, m = 0.5, n = 0.5$.

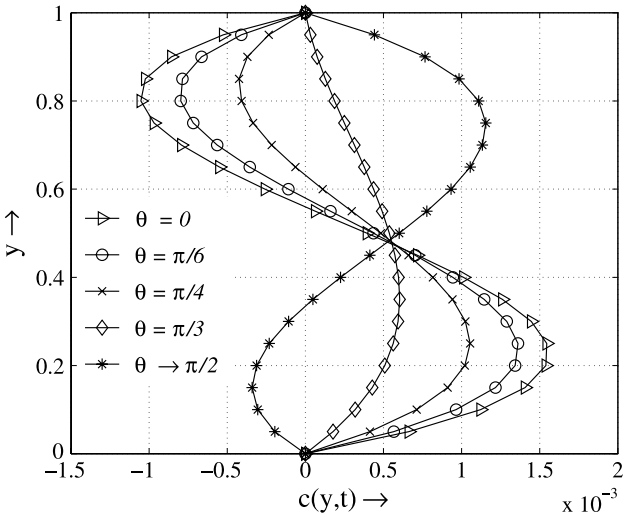

Fig. 16. Effect of θ on $u(y,t)$ for $\alpha = 0.5, R = 0.1, M = 2, \sigma = 5, \Pi_s = \Pi_o = 1, P_j = 1, m = 0.5, n = 0.5$.

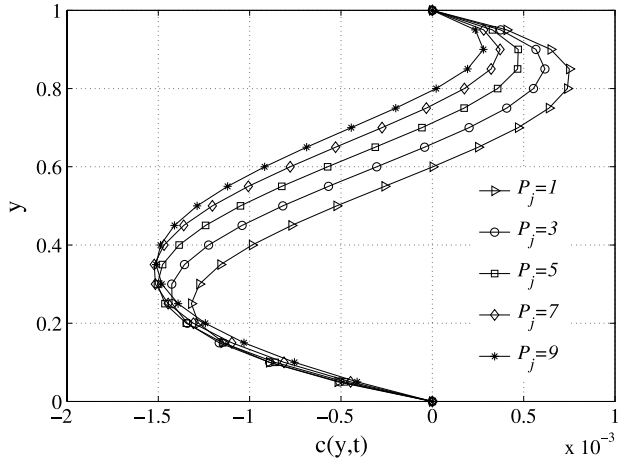

Fig. 17. Effect of P_j on $c(y,t)$ for $\alpha = 0.5, R = 0.1, M = 2, \theta = \pi/6, \sigma = 5, \omega t = \pi/4, \Pi_s =, \Pi_o = 1, m = 0.5, n = 0.5$.

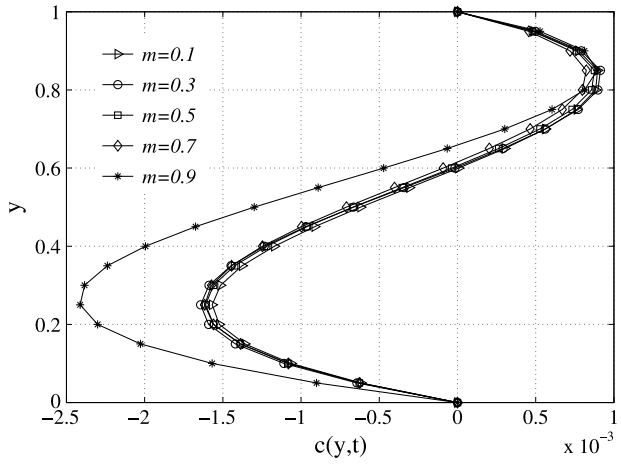

Fig. 18. Effect of m on $c(y,t)$ for $\alpha = 0.5, R = 0.5, M = 1, \theta = \pi/6, \sigma = 5, \omega t = \pi/4, \Pi_s = Pi_o = 1, P_j = 1, n = 0.5$.

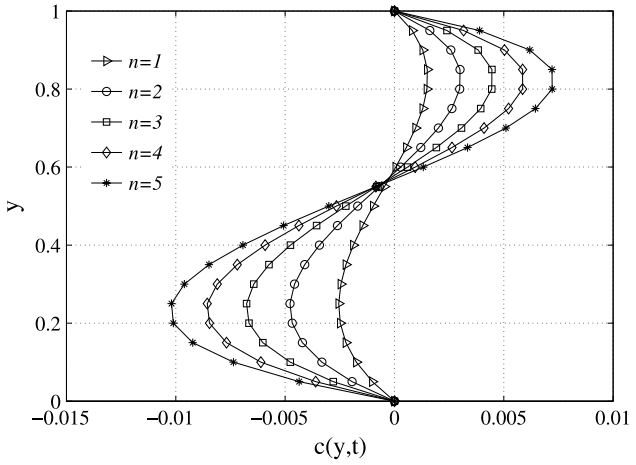

Fig. 19. Effect of n on $c(y,t)$ for $\alpha = 0.5, R = 0.1, M = 2, \theta = \pi/6, \sigma = 5, \omega t = \pi/4, \Pi_s = \Pi_o = 1, P_j = 1, m = 0.5$.

Fig. 17 depicts the variation of microrotation with regard to microinertia parameter P_j. For $0.2 < y < 1.0$, as P_j is increasing, microrotation is decreasing. For $0 < y < 0.2$, as P_j is increasing, microrotation is increasing. From Fig. 18, it is seen that as the coupling parameter m ($0 \leq m < 1$) is increasing, the microrotation is decreasing near the upper permeable bed while it has an increasing trend at the lower permeable bed.

Figs. 19–21 show the variation of microrotation with respect to the gyration parameter n, the porosity parameter σ and the magnitude of the pressure gradient Π_s respectively. We notice that as each of these parameters is increasing, the microrotation is increasing in the region nearer to the upper bed and is decreasing in the region nearer to the lower bed. Fig. 22 shows the variation of microrotation with respect to the magnitude of the oscillatory pressure gradient Π_o. The microrotation is not showing any specific trend with an increase in Π_o.

In Figs. 13–22, the profiles of $c(y,t)$ show a sort of asymmetry about a plane parallel to the beds nearer to the upper permeable bed.

5. Conclusions

In this paper, we have studied the pulsating flow of an incompressible micropolar fluid between two permeable beds under the influence of an inclined uniform magnetic field using Beavers–Joseph (BJ) slip boundary conditions at the interfaces of the permeable beds. Expressions for the velocity and microrotation components are obtained. Their variation is studied numerically and presented through graphs corresponding to the frequency/time parameter ωt, Reynolds number R, inclination angle θ, Hartmann number M, micropolar parameters P_j, m, n, porosity

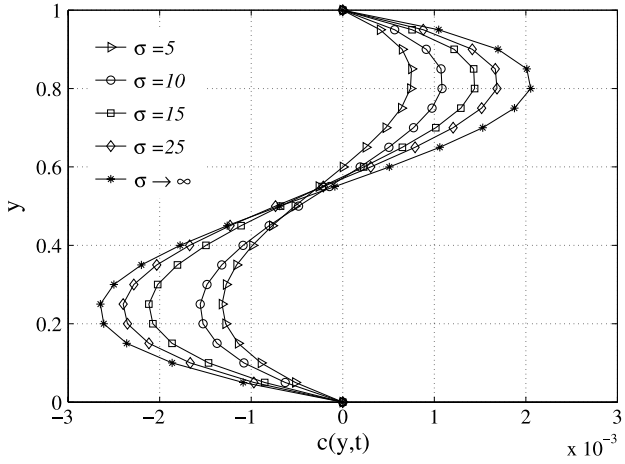

Fig. 20. Effect of σ on $c(y,t)$ for $\alpha = 0.5, R = 0.5, M = 2, \theta = \pi/6, \omega t = \pi/4, \Pi_s = \Pi_o = 1, P_j = 1, m = 0.5, n = 0.5$.

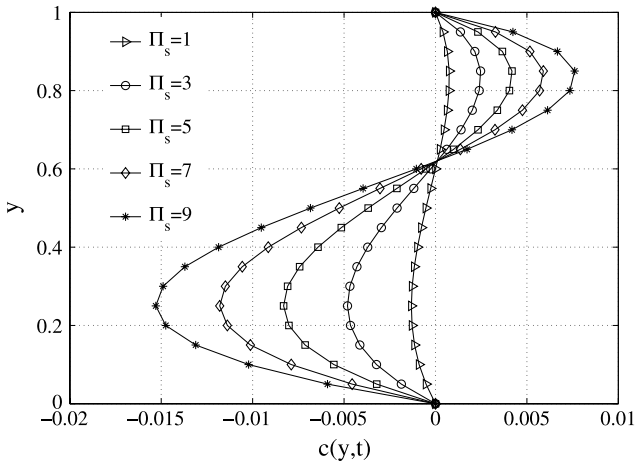

Fig. 21. Effect of Π_s on $c(y,t)$ for $\alpha = 0.5, R = 0.5, M = 2, \theta = \pi/6, \sigma = 5, \omega t = \pi/4, P_j = 1, \Pi_o = 1, m = 0.5, n = 0.5$.

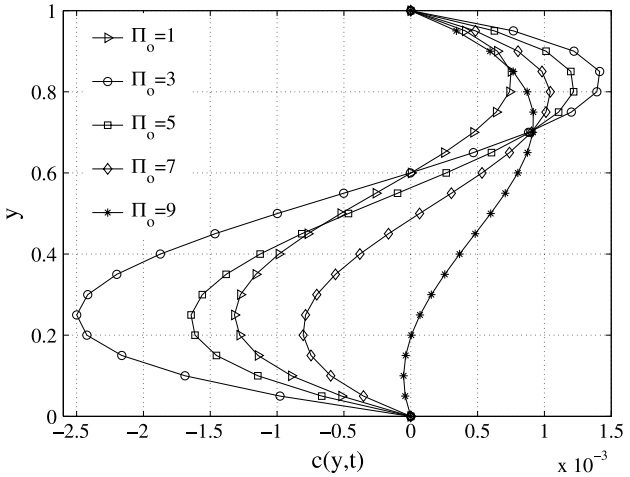

Fig. 22. Effect of Π_o on $c(y,t)$ for $\alpha = 0.5, R = 0.5, M = 2, \theta = \pi/6, \sigma = 5, \omega t = \pi/4, \Pi_s = 1, P_j = 1, m = 0.5, n = 0.5$.

parameter σ and magnitudes of the pressure gradients Π_s, Π_o, by varying one of these parameters and fixing all others. From the results we have the following conclusions.

- The pulsating velocity of the fluid is reduced by the increase of Hartmann number, coupling parameter, porosity parameter and slip parameter.
- Velocity increases by the increase of Reynolds number, inclination angle, microinertia parameter and magnitudes of the steady and oscillatory pressure gradients.
- The microrotation decreases with the increase of microinertia parameter.
- Microrotation is seen to be asymmetric in the flow region about a plane nearer to and parallel to the upper bed.

Acknowledgements

We thank the referees for their comments which have resulted in this revised version of the paper.

Appendix A. Steady part: λ_i's, C_i's and D_i's

$$\lambda_{1,2} = \left(A_s/2 - A_4 \pm \sqrt{A_5 - A_6}\right)/2,$$
$$\lambda_{3,4} = \left(A_s/2 + A_4 \pm \sqrt{A_5 + A_6}\right)/2$$

where

$$A_1 = (B_s^2 + 3A_sC_s + 12D_s),$$
$$A_2 = (2B_s^3 + 9A_sB_sC_s + 27C_s^2 + 27A_s^2D_s - 72B_sD_s)$$
$$A_3 = \sqrt[3]{\frac{A_2 + \sqrt{A_2^2 - 4A_1^3}}{2}}, \qquad A_4 = \sqrt{\frac{A_s^2}{4} - \frac{2B_s + A_3 + A_1/A_3}{3}}$$
$$A_5 = \frac{3A_s^2}{4} - 2B_s - A_4^2, \qquad A_6 = \frac{A_s^3 - 4A_sB_s - 8C_s}{4A_4}$$
$$A_s = R(1 + P_j), \qquad B_s = (R^2P_j + mn - (M\cos\theta)^2 - 2n),$$
$$C_s = R((M\cos\theta)^2P_j + 2n), \qquad D_s = 2n(M\cos\theta)^2$$

and

$$C_1 = \frac{C_2\lambda_2 + C_3\lambda_3 + C_4\lambda_4 - S_1}{\lambda_1}$$
$$C_2 = -\frac{C_3L_{13} + C_4L_{14} + S_1}{L_{12}}$$
$$C_3 = -\frac{T_6 + T_1C_4}{T_2}; \qquad C_4 = \frac{T_2T_5 - T_3T_6}{\Delta_s};$$
$$D_i = \frac{L\lambda_i}{2mn}C_i \quad \text{for } i = 1, 2, 3, 4.$$
$$\Delta_s = T_1T_3 - T_2T_4$$
$$L\lambda_i = (A_s - \lambda_i)\lambda_i^2 - (B_s + 2n)\lambda_i - (M\cos\theta)^2RP_j \quad \text{for } i = 1, 2, 3, 4$$
$$L_{ij} = \left(\lambda_iL\lambda_j - \lambda_jL\lambda_i\right) \quad \text{for } i, j = 1, 2, 3, 4\ (i < j)$$
$$E_{ij} = (e^{\lambda_i} - e^{\lambda_j}) \quad \text{for } i, j = 1, 2, 3, 4\ (i < j)$$
$$El_{ij} = E_{ij}L\lambda_iL\lambda_j \quad \text{for } i, j = 1, 2, 3, 4\ (i < j)$$
$$E\lambda_{ij} = (e^{\lambda_i}\lambda_iL\lambda_j - e^{\lambda_j}\lambda_jL\lambda_i) \quad \text{for } i, j = 1, 2, 3, 4\ (i < j)$$
$$T_1 = \lambda_1\left[\lambda_2E_{12}L_{14} - \lambda_4E_{14}L_{12}\right]$$
$$T_2 = \lambda_1\left[\lambda_2E_{12}L_{13} - \lambda_3E_{13}L_{12}\right]$$
$$T_3 = \lambda_1\left[El_{13}\lambda_2 - El_{12}\lambda_3 - El_{23}\lambda_1\right]$$
$$T_4 = \lambda_1\left[El_{14}\lambda_2 - El_{12}\lambda_4 - El_{24}\lambda_1\right]$$
$$T_5 = \lambda_1El_{12}S_1$$
$$T_6 = \lambda_1\left[(e^{\lambda_1}S_1 - S_2)\lambda_1L\lambda_2 - (e^{\lambda_2}S_1 - S_2)\lambda_2L\lambda_1\right]$$
$$S_1 = -Rs_1 + \alpha\sigma_1u_{sB1}; \qquad Rs_1 = R\Pi_s/[(1 - m)\sigma_1]$$
$$S_2 = Rs_2 - \alpha\sigma_2u_{sB2}; \qquad Rs_2 = R\Pi_s/[(1 - m)\sigma_2]$$
$$u_{sB1} = \frac{F_2F_5 + F_1F_6}{F_2F_4 - F_1F_3}; \qquad u_{sB2} = \frac{F_3F_5 + F_4F_6}{F_2F_4 - F_1F_3}$$
$$F_1 = 1 + \frac{\alpha\lambda_1\sigma_2}{\Delta_s}(T_3H_1 - T_4H_2)$$
$$F_2 = \frac{\alpha\lambda_1\sigma_2}{\Delta_s}(T_3H_4 - T_4H_3)$$
$$F_3 = -1 - \frac{\alpha\sigma_1}{L_{12}}\left[(L\lambda_1 - L\lambda_2) + \frac{\lambda_1}{\Delta_s}H_5\right]$$
$$F_4 = \frac{\alpha\sigma_1}{L_{12}}\left[(e^{\lambda_1}L\lambda_2 - e^{\lambda_2}L\lambda_1) - \frac{\lambda_1}{\Delta_s}H_6\right]$$
$$F_5 = -\frac{R\Pi_s}{M^2} - \frac{1}{L_{12}}\left[Rs_1(e^{\lambda_2}L\lambda_1 - e^{\lambda_1}L\lambda_2) + \frac{\lambda_1}{\Delta_s}H_7\right]$$
$$F_6 = \frac{R\Pi_s}{M^2} + \frac{1}{L_{12}}\left[Rs_1(L\lambda_1 - L\lambda_2) + \frac{\lambda_1}{\Delta_s}H_8\right]$$
$$H_1 = e^{\lambda_4}L_{12} - e^{\lambda_2}L_{14} + e^{\lambda_1}L_{24}$$
$$H_2 = e^{\lambda_3}L_{12} - e^{\lambda_2}L_{13} + e^{\lambda_1}L_{23}$$
$$H_3 = \lambda_3(L\lambda_1 - L\lambda_2) + \lambda_1(L\lambda_2 - L\lambda_3) + \lambda_2(L\lambda_3 - L\lambda_1)$$
$$H_4 = \lambda_4(L\lambda_1 - L\lambda_2) + \lambda_1(L\lambda_2 - L\lambda_4) + \lambda_2(L\lambda_4 - L\lambda_1)$$
$$H_5 = E\lambda_{12}(T_4H_3 - T_3H_4) + El_{12}(T_1H_3 - T_2H_4)$$
$$H_6 = E\lambda_{12}(T_3H_1 - T_4H_2) + El_{12}(T_1H_2 - T_2H_1)$$
$$H_7 = ((Rs_1E\lambda_{12} - Rs_2L_{12})(T_3H_1 - T_4H_2) + El_{12}Rs_1(T_2H_1 - T_1H_2))$$
$$H_8 = ((Rs_1E\lambda_{12} - Rs_2L_{12})(T_4H_3 - T_3H_4) + El_{12}Rs_1(T_2H_4 - T_1H_3)).$$

Appendix B. Unsteady part: λ_i's, C_i's and D_i's

$$\lambda_{5,6} = \frac{1}{2}\left(\frac{A}{2} - A_{o4} \pm \sqrt{A_{o5} - A_{o6}}\right),$$
$$\lambda_{7,8} = \frac{1}{2}\left(\frac{A}{2} + A_{o4} \pm \sqrt{A_{o5} + A_{o6}}\right)$$

where

$$A_{o1} = (B^2 + 3AC + 12D),$$
$$A_{o2} = (2B^3 + 9ABC + 27C^2 + 27A^2D - 72BD)$$
$$A_{o3} = \sqrt[3]{\frac{A_{o2} + \sqrt{A_{o2}^2 - 4A_{o1}^3}}{2}},$$
$$A_{o4} = \sqrt{\frac{A_{o2}}{4} - \frac{2B + A_{o3} + A_{o1}/A_{o3}}{3}}$$
$$A_{o5} = \frac{3A^2}{4} - 2B - A_{o4}^2, \qquad A_{o6} = \frac{A^3 - 4AB - 8C}{4A_{o4}}$$
$$a = (M\cos\theta)^2 + i\omega R, \qquad b = 2n + \omega RP_j,$$
$$A = R(1 + P_j), \qquad B = (R^2P_j + mn - a - b),$$
$$C = R(aP_j + b), \qquad D = ab$$
$$C_8 = \frac{T_{o2}T_{o5} - T_{o3}T_{o6}}{\Delta}; \qquad C_7 = -\frac{T_{o6} + T_{o1}C_8}{T_{o2}};$$
$$C_6 = -\frac{C_7L_{57} + C_8L_{58} + S_{o1}}{L_{56}}$$
$$C_5 = \frac{C_6\lambda_6 + C_7\lambda_7 + C_8\lambda_8 - S_{o1}}{\lambda_5}$$

$$D_i = \frac{L\lambda_i}{mb}C_i \quad \text{for } i = 5, 6, 7, 8.$$

$$\Delta = T_{o1}T_{o3} - T_{o2}T_{o4}$$

$$L\lambda_i = (A - \lambda_i)\lambda_i^2 - (B + b)\lambda_i - RP_j a \quad \text{for } i = 5, 6, 7, 8$$

$$L_{ij} = \left(\lambda_i L\lambda_j - \lambda_j L\lambda_i\right) \quad \text{for } i, j = 5, 6, 7, 8\ (i < j)$$

$$E_{ij} = (e^{\lambda_i} - e^{\lambda_j}) \quad \text{for } i, j = 5, 6, 7, 8\ (i < j)$$

$$El_{ij} = E_{ij}L\lambda_i L\lambda_j \quad \text{for } i, j = 5, 6, 7, 8\ (i < j)$$

$$E\lambda_{ij} = (e^{\lambda_i}\lambda_i L\lambda_j - e^{\lambda_j}\lambda_j L\lambda_i) \quad \text{for } i, j = 5, 6, 7, 8\ (i < j)$$

$$T_{o1} = \lambda_5\left[\lambda_6 E_{56}L_{58} - \lambda_8 E_{58}L_{56}\right]$$

$$T_{o2} = \lambda_5\left[\lambda_6 E_{56}L_{58} - \lambda_7 E_{57}L_{56}\right]$$

$$T_{o3} = \lambda_5\left[El_{57}\lambda_6 - El_{56}\lambda_7 - El_{67}\lambda_5\right]$$

$$T_{o4} = \lambda_5\left[El_{58}\lambda_6 - El_{56}\lambda_8 - El_{68}\lambda_5\right]$$

$$T_{o5} = \lambda_5 El_{56}S_{o1}$$

$$T_{o6} = \lambda_5\left[(e^{\lambda_5}S_{o1} - S_{o2})\lambda_5 L\lambda_6 - (e^{\lambda_6}S_{o1} - S_{o2})\lambda_6 L\lambda_5\right]$$

$$S_{o1} = -Rs_{o1} + \alpha\sigma_1 u_{oB1}; \qquad Rs_{o1} = R\Pi_o/[(1 - m)\sigma_1]$$

$$S_{o2} = Rs_{o2} - \alpha\sigma_2 u_{oB2}; \qquad Rs_{o2} = R\Pi_o/[(1 - m)\sigma_2]$$

$$u_{oB1} = \frac{G_2G_5 + G_1G_6}{G_2G_4 - G_1G_3}; \qquad u_{oB2} = \frac{G_3G_5 + G_4G_6}{G_2G_4 - G_1G_3}$$

$$G_1 = 1 + \frac{\alpha\lambda_5\sigma_2}{\Delta}(T_{o3}K_1 - T_{o4}K_2)$$

$$G_2 = \frac{\alpha\lambda_5\sigma_2}{\Delta}(T_{o3}K_4 - T_{o4}K_3)$$

$$G_3 = -1 - \frac{\alpha\sigma_1}{L_{56}}\left[(L\lambda_5 - L\lambda_6) + \frac{\lambda_5}{\Delta}K_5\right]$$

$$G_4 = \frac{\alpha\sigma_1}{L_{56}}\left[(e^{\lambda_5}L\lambda_6 - e^{\lambda_6}L\lambda_5) - \frac{\lambda_5}{\Delta}K_6\right]$$

$$G_5 = -\frac{R\Pi_o}{a} - \frac{1}{L_{56}}\left[Rs_{o1}(e^{\lambda_6}L\lambda_5 - e^{\lambda_5}L\lambda_6) + \frac{\lambda_5}{\Delta}K_7\right]$$

$$G_6 = \frac{R\Pi_o}{a} + \frac{1}{L_{56}}\left[Rs_{o1}(L\lambda_5 - L\lambda_6) + \frac{\lambda_5}{\Delta}K_8\right]$$

$$K_1 = e^{\lambda_8}L_{56} - e^{\lambda_6}L_{58} + e^{\lambda_5}L_{68}$$

$$K_2 = e^{\lambda_7}L_{56} - e^{\lambda_6}L_{57} + e^{\lambda_5}L_{67}$$

$$K_3 = \lambda_7(L\lambda_5 - L\lambda_6) + \lambda_5(L\lambda_6 - L\lambda_7) + \lambda_6(L\lambda_8 - L\lambda_5)$$

$$K_4 = \lambda_8(L\lambda_5 - L\lambda_6) + \lambda_5(L\lambda_6 - L\lambda_8) + \lambda_6(L\lambda_8 - L\lambda_5)$$

$$K_5 = E\lambda_{56}(T_{o4}K_3 - T_{o3}K_4) + El_{56}(T_{o1}K_3 - T_{o2}K_4)$$

$$K_6 = E\lambda_{56}(T_{o3}K_1 - T_{o4}K_2) + El_{56}(T_{o1}K_2 - T_{o2}K_1)$$

$$K_7 = ((Rs_{o1}E\lambda_{56} - Rs_{o2}L_{56})(T_{o3}K_1 - T_{o4}K_2) + El_{56}Rs_{o1}(T_{o2}K_1 - T_{o1}K_2))$$

$$K_8 = ((Rs_{o1}E\lambda_{56} - Rs_{o2}L_{56})(T_{o4}K_3 - T_{o3}K_4) + El_{56}Rs_{o1}(T_{o2}K_4 - T_{o1}K_3))$$

References

[1] M. Zamir, The Physics of Pulsatile Flow, Springer-Verlag, New York, 2000.
[2] M.O. Carpinlioglu, M.Y. Gundogdu, A critical review on pulsatile pipe flow studies directing towards future research topics, Flow Meas. Instrum. 12 (2001) 163–174.
[3] Y.C. Wang, Pulsatile flow in a porous channel, J. Appl. Mech. 38 (1971) 553–555.
[4] K. Vajravelu, K. Ramesh, S. Sreenadh, P.V. Arunachalam, Pulsatile flow between permeable beds, Int. J. Non-Linear Mech. 38 (2003) 999–1005.
[5] T. Malathy, S. Srinivas, Pulsating flow of a hydromagnetic fluid between permeable beds, Int. Commun. Heat Mass Transfer 35 (2008) 681–688.
[6] K. Ramakrishnan, K. Shailendhra, Hydromagnetic flow through uniform channel bounded by porous media, Appl. Math. Mech. (English Edition) 32 (7) (2011) 837–846.
[7] K. Avinash, J. Anada Rao, S. Sreenadh, Y.V.K. Ravikumar, Pulsatile flow of a viscous stratified fluid of variable viscosity between permeable beds, J. Porous Media 14 (12) (2011) 1115–1124.
[8] T.K.V. Iyengar, B. Punnamchandar, Pulsating flow of an incompressible couple stress fluid between permeable beds, World Academy of Science, Engineering and Technology 5 (8) (2011) 1180–1190.
[9] B. Punnamchandar, T.K.V. Iyengar, Pulsating flow of an incompressible micropolar fluid between permeable beds, Nonlinear Anal. Model. Control 18 (4) (2013) 399–411.
[10] A.C. Eringen, Theory of micropolar fluids, J. Math. Mech. 16 (1966) 1–18.
[11] A.C. Eringen, Microcontinuum Field Theories II: Fluent Media, Springer-Verlag Press, New York, 1998.
[12] G. Lukaszewicz, Micropolar Fluids: Theory and Applications, Birkhauser, Boston, 1999.
[13] G.S. Beavers, D.D Joseph, Boundary conditions at a naturally permeable wall, J. Fluid Mech. 30 (1967) 197–207.
[14] E.M. Sparrow, R.D. Cess, Magnetohydrodynamic and heat transfer about a rotating disk, J. Appl. Mech. 29 (1962) 181–187.
[15] P.A. Davidson, An Introduction to Magnetohydrodynamics, Cambridge University Press, New York, 2001.